Biomineralization of magnetic nanoparticles in stem cells

Alexandre Fromain, Aurore van de Walle, Guilhem Curé, Christine Péchoux, Aida Serrano, Yoann Lalatonne, Ana Espinosa, Claire Wilhelm

Biomineralization of magnetic nanoparticles in stem cells

Alexandre Fromain [a+], Aurore Van de Walle [a+], Guilhem Curé [a], Christine Péchoux [b], Aida Serrano [c], Yoann Lalatonne [d], Ana Espinosa [e], Claire Wilhelm [a] *

Iron is one of the most common metals in the human body, with an intrinsic metabolism including proteins involved in its transport, storage, and redox mechanisms. A less explored singularity is the presence of magnetic iron in the organism, especially in the brain. The capacity of human stem cells to biosynthesize magnetic nanoparticles was recently demonstrated, yet using iron released by the degradation of synthetic magnetic nanoparticles. To evidence a magnetic biomineralization in mammalian cells, it is needed to address the biosynthesis of magnetic nanoparticles in cells supplied exclusively with non-magnetic iron salt precursors. Herein mouse and human mesenchymal stem cells were incubated with ferric quinate for up to 36 days. By optimizing concentration and culture time, and by measuring both total intracellular iron content and cellular magnetic signal, the biosynthesis of magnetic nanoparticles was observed to happen from 14 days of continuous iron incubation, and correlated with important doses of intracellular iron. Local electronic structure and chemical environment of intracellular iron was further dissected with XAS spectroscopy at the Fe K-edge, showing a total conversion of Fe^{2+} to Fe^{3+} when using ferrous salts (ascorbate and sulfate), and a transformation towards ferrihydrite with a small proportion of magnetic phase.

Introduction

Iron is one of the most preeminent metals on earth and is part of the few metals involved in human metabolism.[1] More specifically, this transition metal can undergo oxidation and reduction processes and, remarkably, do so within the entire redox potential of living systems, being approximately between -400 and +800 mV at pH 7. The implications are quite extraordinary as, with only one metal, it is possible to carry out biochemical reactions within almost 1 V of redox potential by modulating the coordination of iron (e.g. linked to sulfur in Fe-S clusters or cytochromes).[2] Despite acknowledging the presence of iron in cells as well as proteins and transporters associated to the regulation of this metal, cell behavior in presence of iron is not yet fully dissected. Besides, iron-based nanomaterials remain leading actors in the nanomedicine field for theranostics approaches.[3-14]

One of the singularities still poorly understood regarding iron in the human body consists in its presence under a magnetic form. It has been shown since the 1990's that iron oxides nanoparticles, which are magnetic, are present in various organs such as the brain.[15, 16] Their provenance can be attributed to our polluted environment, with magnetic nanocrystals being released from brake wear for instance.[17] A biological origin has also long been suggested,[18] but experiment evidence was still missing. Recently, it was demonstrated that human stem cells are indeed capable of the bioproduction of magnetic nanoparticles.[19, 20] Rather, this was only an indirect evidence as the magnetic biosynthesis reported was achieved after internalization of iron oxide nanoparticles, synthesized chemically. Iron, coming from the degradation of these synthetic nanoparticles, was recrystallized by the human cells, corresponding to the synthesis of magnetic nanoparticles anew. This indirect proof nevertheless strongly suggested that human stem cells are capable of performing biogenic magnetic synthesis from iron ions.

Besides, this certainly recalls biomineralization by microorganisms. For instance, cells of bacteria, fungi, and plants were described to successfully biomineralize nanoparticles[21] (e.g. gold,[22, 23] silver,[24] or magnetite[25, 26]). In particular, the magnetite biosynthesis reported in microorganisms has been extensively studied within the magnetotactic bacteria, for which numerous genes encoding for specific proteins have been described as being part of the magnetic biosynthesis mechanism.[27] The properties of these biosynthesized magnetic nanoparticles, called magnetosomes,[28, 29] can also be tuned by using and combining recombinant proteins extracted from the magnetotactic bacteria in E coli.[30] For such biomineralization processes, the biosynthesis is systematically achieved by feeding the microorganisms with non-magnetic iron salts only. Moreover, some of the magnetotactic bacteria genes, such as MagA or mms6, were transfected within mammalian cells, which successfully replicated the biomineralization process leading to the formation of magnetic nanoparticles.[31-33] By contrast, experimental evidences of biogenic intracellular nanoparticles synthesis by mammalian cells remain scarce. Some works described multi-element biosynthesis of nanoclusters,[34-37] in the 3 nm range, yet limited to cancer cells, due to their enhanced reducing activity.

Nevertheless, as mentioned before, the biosynthesis of magnetic nanoparticles, in the 6-8 nm range was recently evidenced in mesenchymal stem cells, but using the ionic species delivered by the full degradation of chemically synthetized nanoparticles. The goal of this work was to explore if this biosynthesis could happen from iron salt precursors only. To do so, mouse and human mesenchymal stem cells (mMSC and hMSC) were continuously incubated with iron salts for up

[a.] *Laboratoire Physico Chimie Curie, CNRS UMR168, Institut Curie, Sorbonne Université, PSL University, 75005 Paris, France.*
[b.] *Université Paris-Saclay, INRAE, AgroParisTech, GABI, 78350, Jouy-en-Josas, France.*
[c.] *Departamento de Electrocerámica, Instituto de Cerámica y Vidrio, ICV-CSIC, C/ Kelsen 5, 28049 Madrid, Spain*
[d.] *Université Sorbonne Paris Nord, Université Paris Cité, Laboratory for Vascular Translational Science, LVTS, INSERM, UMR 1148, Bobigny F-93017, France; Département de Biophysique et de Médecine Nucléaire, Assistance Publique-Hôpitaux de Paris, Hôpital Avicenne F- 93009 Bobigny, France.*
[e.] *IMDEA Nanociencia, C/ Faraday 9, 28049 Madrid, Spain; Instituto de Ciencia de Materiales de Madrid, Consejo Superior de Investigaciones Científicas, calle Sor Juana Inés de la Cruz 3, 28049 Madrid, Spain*
+ Equal contribution
* Address correspondence to claire.wilhelm@cnrs.fr

to 36 days. Next, the objectives were to identify the kinetics of magnetic nanoparticles occurrence, assess the impact of the dose (with administered iron concentration varied between 10 µM to 1 mM), and evaluate the role of iron supply (ferric quinate, ferrous sulfate, and ferrous ascorbate were used in the culture medium). The presence of citrate as chelating agent was also investigated. From a biological viewpoint, cellular management of high doses of internalized iron was assessed (viability and iron metabolism gene expression). Further, from a physico-chemical viewpoint, iron was fully monitored in cells using Fe K-edge X-ray absorption spectroscopy (XAS) over the whole biosynthesis period.

Results

Magnetic biomineralization in mMSCs upon continuous exposure to Fe^{3+} ions (Ferric Quinate)

mMSC were incubated with ferric quinate at [Fe] = 34 µM = C_0 over 36 days. This C_0 (34 µM) condition was selected to match the biomineralization process in magnetotactic bacteria, generally fed with ferric quinate at this concentration.[38] At specific time points corresponding to days 0, 3, 7, 14, 21, 28, and 36, cell samples were harvested, counted, and investigated by elemental analysis (ICP-AES) and magnetometry (VSM) to determine total iron per cell and magnetization, respectively. Cell number slowly increased over time (Figure 1A), consistent with the fact that they were initially seeded at a high degree of confluence, together with their stem cells nature allowing them to mature in a dense monolayer with a slowing down of cell division. Total iron measurements indicated an increased internalization of iron over time (Figure 1B). VSM analyses performed on cell bulks revealed the appearance of a magnetic signal, with super-paramagnetic signature (Figure 1C and 1D), detectable after 14-21 days of incubation. Magnetization curves (n=12) were fitted to Langevin law weighted with lognormal size distribution to extrapolate the diameter and polydispersity of the magnetic nanostructures. It revealed an average magnetic diameter of d_{mag}=6.6±0.8 nm and a polydispersity index of σ=0.36±0.05. The average magnetic moment at saturation could also be extracted from the VSM curves at each time point (Figure 1E), corresponding to the values for the entire cell samples (the 200 000 cells initially seeded at day 0), found in the range of 4-10 $x10^{-6}$ emu (µemu). It corresponds to cellular magnetic moments in the 2-4 $x10^{-12}$ emu (~pemu) range (obtained by simply normalizing the magnetic moment by the number of cells indicated in Figure 1A). The emu per grams of Fe can also be directly inferred by dividing the saturation magnetic moment of each sample by the total iron content as measured by ICP. These values, frequently used to characterize a magnetic sample, are shown in Figure 1F. Clearly, cell magnetization remains low, with values in the 1 emu/g_{Fe} range only. Nevertheless, it is the evidence of a magnetic biomineralization that takes place upon a minimum of 14 days of culture, when the stem cells are loaded with iron.

Transmission Electron Microscopy (TEM) imaging of 70 nm-thick sections of cells along their continuous culture with 34 µM ferric quinate showed the presence of 5-7 nm nanoobjects typical of ferritin loaded with iron since the first days of incubation, and mostly within intracellular endosomes (Figure 2A-D). This is consistent with the endocytotic import of Fe^{3+} by transferrin, capable of binding two Fe^{3+} atoms and interacting with the cell surface transferrin receptor (TfR). Systematic size measurement on TEM images of the observed nanostructures showed an average particle diameter around 6 nm, with no statistical differences over time (Figure 2E). As expected, this size fits the internal diameter of the ferritin protein, responsible for iron storage within the cell and known to have a 6-8 nm core.[39] This protein is made of two types of subunits, light (L) and heavy (H), with varying ratios depending on cell type. The H-subunit has a ferroxidase activity and is responsible for the conversion of iron from its ferrous (Fe^{2+}) to its ferric (Fe^{3+}) form, while the L-subunit is responsible for electron transfer across the protein cage.

Next step was then to quantify the expression of the genes coding for these subunits (Figure 2F-I). It showed a progressive increase of both L (Figure 2F) and H (Figure 2G) subunits gene expression over time, with the H-subunit being 20-fold upregulated at day 36, while upregulation of the L subunit was only 10-fold. Genes coding for transferrin receptor that regulate intracellular iron import (Figure 2H) and ferroportin that regulate its export (Figure 2I) were also upregulated; however, it was only 6-fold for transferrin receptor and 4-fold for ferroportin at day 36. Interestingly, there was no balance shift indicating only an export of iron, which could have been expected following a continuous incubation with iron. Instead, iron import seems to keep on taking place at day 36, which is consistent with iron internalization data (Figure 1), which does not markedly saturate at day 36. Moreover, iron incubation does not appear cytotoxic as indicated by the proliferation data from Figure 1A and by the metabolic activity of cells initially loaded with 2 pg of iron per cell via a 1 mM ferric quinate incubation for 24h and kept in culture for 36 days (Figure 2J).

Magnetic biomineralization with Ferric Quinate is similar in hMSCs.

Ferric quinate incubation was also performed on human mesenchymal stem cells (hMSC), over their differentiation along the adipogenic pathway (Figure 3). Indeed, in hMSC, adipogenesis was shown as the most efficient differentiation pathway for the neo-production of biomagnetic nanoparticles in the initial re-magnetization experiments. Magnetization curves were obtained for cell samples corresponding to an initial seeding of 200 000 cells, as it was done with mMSCs (Figure 3C). Remarkably, similar average values of the magnetic moment at saturation were obtained for hMSCs (Figure 3D) compared with mMSCs (Figure 1E), in the 2-8 µemu for the global cell samples. Logically, the size of the nanostructures observed on TEM images (Figure 3A at day 21 and Figure 3B at day 36), showed an average diameter around 6 nm, without

significant difference over time (Figure 3E), exactly the same situation as for the mMSCs (Figure 2E).

Effect of extracellular dose of Ferric Quinate on biomineralization

In the first part of this study, iron incubations were achieved with ferric quinate at iron concentration of 34 µM (defined as C_o), as it is the most used condition for iron culture with magnetotactic bacteria. The effect of dose yet needed to be explored in mammalian cells. Additional incubation doses, ranging from $0.5C_o$ ([Fe]=17 µM) to $16C_0$ ([Fe]=544 µM), were tested on mouse MSC (mMSC). Following 36 days of continuous iron supplementation with these different iron doses, without or with citrate (2 mM), cell number, total iron internalized by the cells and cellular biomagnetism were measured (Figure 4). Increased iron dose does not impact mMSC proliferation, which is however lower in the presence of citrate (Figure 4A compared to 4B). Clearly an increase in iron dose increases the amount of internalized iron, both with and without citrate (Figure 4C and 4D), yet the magnetic biosynthesis happens to not necessarily correlate with such increase, especially in presence of citrate (Figure 4E-H). The total biomineralization expressed in µemu for the entire cell sample (always starting from the same amount of 200 000 cells, Figures 4E and 4F) was similar with or without citrate at low doses, but was 10-fold higher with citrate at high dose ($16C_0$). When renormalizing this magnetic moment with the number of cells at 36 days, the cellular magnetization was systematically higher with citrate (Figure 4G and 4H) reaching the highest value of 6 pemu per cell at $16C_0$.
Nevertheless, despite the role of citrate in cell proliferation, the magnetization remained relatively consistent with and without citrate, as shown by the renormalized emu per gram of Fe values presented in Figures 4I and 4J. Although slight differences were observed at the doses of 0.5Co (where citrate improved performance) and Co and 2Co (where citrate reduced performance), both conditions yielded a significantly lower rate of magnetic biosynthesis at high concentrations. Increasing the dose was thus not beneficial for magnetic biosynthesis, and the C_0 dose used with microorganism appears to be the most efficient one.

In situ EXAFS/XANES investigation of iron local atomic structure during biomineralization

The short-range structure and coordination of iron within the cellular environment were monitored over time using XAS technique.[40] XAS spectra at the X-ray absorption near-edge structure (XANES) and extended X-ray absorption fine structure (EXAFS) regimes were measured at the Fe K-edge (7112 eV). Spectra of iron-loaded cells along their culture were determined in fluorescence mode and compared with initial iron-based precursors in solution and with reference samples, γ-Fe_2O_3 (maghemite), $Fe_2O_3{\cdot}0.5H_2O$ (ferrihydrite)). *In situ* biomineralization of ferric quinate salt was first assessed upon 36 days of continuous salt supplementation (Figure 5A). Clearly, the iron valence Fe^{3+} is perfectly maintained from the iron salt solution to the final maturation in cells after 36 days. To check if this was imposed by the initial iron state (Fe^{3+} vs. Fe^{2+}), two additional iron salts were also tested, either ferrous ascorbate (Figure 5B) or Mohr's salt (Figure 5C), both with Fe^{2+} valence. Remarkably, for both salts, a total change of iron valence toward Fe^{3+} is evidenced. The position of the edge in the XANES spectrum is linked to the formal valence of a metal.[41] Hence, XANES analysis can be performed by utilizing linear combinations of established reference spectra to determine the compositional fractions of the various components present. In this case, the XANES spectra in cells at D36 can be simulated considering ferrihydrite and magnetic iron oxides in less proportions together with Fe-based compounds combined with elements present in the cellular environment (P, S, Ca...). The signal obtained for biomineralized intracellular iron at 36 days almost perfectly fits the one of ferrihydrite for iron sources. Yet, it fully fits the ferrihydrite signal only when incubated with Mohr's salt, while for the two other salts (ferric quinate and ferrous ascorbate), the signals match one of ferrihydrite accompanied with small proportion of iron oxides. It thus validates the small magnetic biosynthesis observed at 36 days of continuous incubation with ferric quinate.
From EXAFS analysis (Figure 5D-5F), one shell is located around 2.0 Å in three salt solutions which is associated with the distance of Fe cations to the first atomic neighbors. In all three cases, the position of first neighbors falls at longer distances than the first shell corresponding to the ferrihydrite and maghemite references associated with Fe-O bonds. Spectra of iron-loaded upon 36 days show a change in the EXAFS signal related to the compositional and structural modification. EXAFS spectra of cells display the first shell at shorter distances than in salt solutions and close to that of maghemite or ferrihydrite. In addition, after the maturation in cells of 36 days, the presence of a second shell is located around 2.9 Å that can be related to Fe-Fe distances (although with very low intensity), indicating the biomineralization of salts. This low signal from the excipient second shell, together with the XANES data, indicate that this effect may be associated with a phase created with a more amorphous character than references.

To finally explore the first events of iron management by the cells, XAS analyses were also achieved after 5 hours of iron salts administration, and along one week afterwards (Figure 6). Yet, to have a sufficient signal, iron dose was increased to [Fe]=4 mM, and cells were exposed for 7 hours only to avoid toxicity. Images of the cells pellets for all three salts are shown in Figure 6A-6C, revealing a marked coloring of the samples over time. Interestingly, it reveals that the change of iron valence toward Fe^{3+} for (Fe^{2+}) ferrous ascorbate (Figure 6E) and Mohr's salts (Figure 6F) has already happened at 5 hours of cell internalization, with no major changes after one day or one week of cells maturation.

Discussion and Conclusion

The recent evidence that human stem cells are able to reshape magnetic nanoparticles, from synthetic or biological origin, into new magnetic nanoparticles, produced directly by the human cells, opened up to the question of a possible totally biological synthesis, using iron ions only as precursors. Indeed, magnetic crystals have been identified in several organisms, including the

magnetotactic bacteria, probably the most studied and understood. This group of bacteria can sense and align along the geomagnetic field via the biosynthesis of highly organized magnetic nanoparticles named magnetosomes. Fishes, mollusks, birds, honey bees, and even humans have also been shown to possess such magnetic crystals;[42] In humans, they have been localized in specific organs such as the brain and heart of patients.[43, 44] The reason behind their presence is however still debated. They could be a remaining evolutionary feature allowing us to sense the geomagnetic field, as it has recently been demonstrated that Earth-strength magnetic fields do affect human alpha brain waves.[45] Several hypotheses have been emitted regarding magnetic nanoparticles as magnetoreceptors.

In this work, iron management and biomineralization were explored in mouse and human mesenchymal stem cells (MSC). MSC were selected based on the results of initial investigations using exogenous magnetic nanoparticles as an iron precursor.[19] These studies were conducted in human MSCs and demonstrated that the biosynthesis of magnetic nanoparticles occurred in this cell type. Interestingly, this phenomenon appeared to be specific to certain cell types, as human umbilical vein endothelial cells (HUVECs) did not exhibit the ability to biosynthesize magnetic nanoparticles under the same conditions.[20] Here, mMSCs and hMSCs were incubated with ferric quinate at varying doses and results emphasize iron biomineralization and the formation of magnetic crystals. With such setup, cells progressively internalize iron over time and magnetic cells are obtained following a relatively long culture, as it requires over 21 days for the human stem cells and 14 days for the mouse ones before reaching detectable magnetism values. It is much longer than for the magnetic nanoparticles biosynthesized upon the degradation of exogenous ones, which are detectable after only 9 days of culture.[19, 20] Moreover, resulting magnetization values are lower with iron ion precursors. This could be explained by the slower internalization of the iron ion precursors in comparison to the nanoparticle ones, which are more readily and efficiently endocytosed. Indeed, incubation of these same cells for 24h with 1 mM nanoparticles results in 10 pg of iron per cell (data not shown), while a 24h incubation with 1 mM ferric quinate results in only 2 pg of iron per cell.

Even if the resulting magnetization values remain low, it is the proof-of-concept that such a biosynthesis is possible. The results also provide evidence of the cells' ability to withstand sustained iron incubations while maintaining viability. Our previous observations of biosynthesis using iron oxide nanoparticles as iron precursor suggest that this process occurs through differentiation pathways that are not impacted by high iron loads. Thus, we hypothesized that the biosynthesis of magnetic nanoparticles may serve as a detoxification mechanism in response to high intracellular iron doses. Besides, the role of chelating agent (here citrate) is evidenced. Citrate is a molecule intertwined with iron metabolism in mammals as, to avoid adverse effects due to free iron ions such as Fenton reaction and the production of reactive oxygen species (ROS), or again to impede precipitation of Fe^{3+} as $Fe(OH)_3$, Fe^{3+} can complex with citrate.[46] Its presence has been reported in human blood plasma in concentrations of 0.1 mM, and it has been shown as an important iron ligand in patients suffering from iron overload.[46] Herein, the supplementation with citrate (2 mM) had a direct effect on cell growth, decreasing proliferation. Similar observations have been made in cancer cells; studies described a mitochondria-mediated apoptosis induced by high citrate concentration.[47, 48] Citrate also resulted in higher magnetic moment per cell after 36 days of continuous incubation at high dose (16 C_o).

These results show an overexpression of both the light (L) and heavy (H) chains of the ferritin protein, which is responsible for iron storage within cells. We hypothesize that the biosynthesis of magnetic nanoparticles occurs within the core of ferritin, which has a diameter of 6 to 8 nm. This is supported by previous research showing that magnetoferritin can be chemically produced by filling the ferritin core with an iron oxide crystal.[49, 50] Interestingly, the overexpression of both ferritin chains (H and L) observed in this study contrasts with the results from the biosynthesis experiments based on magnetic nanoparticles, where only the H-subunit was overexpressed, leading us to initially hypothesize that this subunit, which possesses ferroxidase activity and is typically used as a supporting structure by chemists for magnetoferritin formation, may initiate the biosynthesis process. However, it is important to note that, when starting from non-magnetic iron salt, a large proportion of iron remained stored as ferrihydrite (non-magnetic), which may explain the overexpression of both ferritin subunits (with L mostly driven by ferrihydrite storage and H encouraging storage under a magnetic form, such as magnetite or maghemite).

XANES and EXAFS experiments were performed at the Fe K-edge to qualitatively investigate the valence states and local structural properties of the metal Fe cations and the ferrite phases over the biomineralization process. XANES is a sensitive probe of the coordination and oxidation state of absorbing ions and EXAFS gives information about their local environment, including interatomic distances and coordination numbers of surrounding shells. These two complimentary techniques, considered non-damaging, can thus reveal the short-range geometry and identify the phases.[20, 51] Analyses were performed after 36 days of culture with continuous iron supplementation and upon a few hours of iron supply at 100-fold higher dose. Besides, other salt with initial Fe^{2+} valence (ferrous ascorbate and Mohr's salt) were investigated at the same doses and incubation time. Remarkably, for all three salts and all times analyzed (5 hours, day 1, day 7, day 36), iron is under the oxidation state 3+ on average. Besides, the signals were very similar whatever the salts, with strong correlation with ferrihydrite after 36 days of mineralization. Interestingly, during the first days of internalization, it was less consistent with ferrihydrite, maybe revealing a proportion of Fe^{3+} ions with other different coordination, possibly linked to small molecules such as citrate for instance. Overall, these data demonstrate that iron is predominantly under the Fe^{3+} oxidation state once within the cells, even with the Fe^{2+} ferrous ascorbate and

Mohr's salt incubations, and that this transformation takes place on short times (~hours).

To conclude, an approach for intracellular bioinorganic magnetic nanoparticles synthesis is evidenced in stem cells, upon administration of non-magnetic iron salts exclusively, using only the internal machinery of mammalian cells to biomineralize iron. It could have direct fundamental impact on bioinorganic chemistry and nanomedicine, transposing bio-inspired strategies within the ultimate intracellular environment with highest complexity and delivering 100% biological magnetic nanoparticles; together with an environmental impact to understand the causes and origins of magnetic nanoparticles presence in the human body.

Experimental

Stem cell culture

Murine mesenchymal stem cell (mMSC) line C3H/10T1/2, Clone 8 (ATCC CCL-226) were cultured in DMEM medium supplemented with 10% FBS and 1% penicillin streptomycin (Thermo Fischer Scientific) at 37 °C with 5% CO_2. Cells were grown until passage 10 to 25 and at 80% confluence prior to seeding.

Human mesenchymal stem cells (hMSC, Lonza) were cultured in MSCGM medium (Lonza) at 37 °C with 5% CO_2. hMSCs were grown until passage 5 to 6 and at 80% confluence prior to seeding. They were subjected to adipogenic differentiation, which was shown as the most efficient differentiation pathway (when compared to osteogenesis and chondrogenesis, or to keeping the MSC in an undifferentiated state) for the neo-production of biomagnetic nanoparticles in the initial re-magnetization experiments(3). Cells were seeded in six-well plates ($2x10^5$ cells/well) and their adipogenic differentiation was induced as previously described (3). Briefly, two independent media were used. First, cells were cultured in Adipogenic Induction Medium (AIM) that consisted of high glucose DMEM (Dulbecco's Modified Eagle Medium) (Thermo Fischer Scientific) supplemented with 10% FBS, 1% penicillin and streptomycin (Thermo Fischer Scientific), 10 ng/mL insulin (Sigma), 1 µM dexamethasone (Sigma), 200 µM indomethacin (Sigma), and 500 µM isobutyl methylxanthine (Sigma). After three to four days, medium was changed to Adipogenic Differentiation Medium (ADM) for three days, which was composed of high glucose DMEM supplemented with 10% FBS, 1% penicillin-streptomycin, and 10 ng/mL insulin. The treatment was repeated three times (AIM for three to four days followed by ADM for three days) then cells were maintained in ADM until day 36, with media replenished twice a week.

Incubation with Ferric Quinate, Ferrous Ascorbate, or Ferrous Sulfate (Mohr's Salt)

Cells were seeded in six-well plates ($2x10^5$ cells/well) and, the following day, were incubated with three types of iron salts that vary in the valence state of their iron ions, being Fe^{3+} for ferric quinate while Fe^{2+} for ferrous ascorbate and ferrous sulfate known as Mohr's salt. Iron solutions were prepared maximum 10 minutes prior use. Stock solutions were prepared in water, in conditions where they are kept soluble, as follows: 270 mg iron(III) chloride hexahydrate (Sigma) with 190 mg D-quinic acid (Sigma) diluted in 10 mL distilled H_2O for the 100 mM ferric quinate stock; 406 mg iron ascorbate (Sigma) diluted in 10 mL distilled H_2O for the 100 mM ferrous ascorbate stock, and 392 mg ammonium iron(II) sulfate hexahydrate (Sigma) diluted in 10 mL distilled H_2O for the 100 mM Mohr's salt stock. Solutions were 0.2 µm filtered before dilution in cellular medium. Typical working iron concentration was defined as C_0 = 34µM. Other concentrations were tested, within two ranges: a low one, from [Fe] = 17 µM ($0.5C_0$) to [Fe] = 544 µM ($16C_0$), and a higher one, at 1, 2, 3, and 4 mM. All solutions were incubated at 37 °C and 5% CO_2 without or with the addition of citrate (Sigma), at 2 mM. Incubation was generally continuous for up to 36 days for the $0.5C_0$, C_0, $2C_0$, $4C_0$, and $16C_0$ conditions. Yet, to explore the short term internalization of iron, incubation at [Fe] = 4 mM was also conducted but for 7 hours only, and with medium containing iron changed every hour. For the continuous incubations, iron salts and citrate were added at each medium change (twice a week).

Iron quantification

For each sample, cell number was counted using a counting chamber (Malassez) and samples were digested in 290 µL of 69% nitric acid (Sigma). Upon minimum two days of digestion, samples were diluted in filtered ultrapure water such as obtaining a final solution at 2% nitric acid. Total iron content was measured by inductively coupled plasma – Atomic Emission Spectroscopy (ICP-AES) (Spectrogreen, SPECTRO, Germany), and reported to the number of cells.

Samples Magnetometry

Cells were counted using a Malassez chamber and samples were fixed in 4% paraformaldehyde then rinsed in phosphate-buffered saline (PBS). Magnetism values of fixed samples were analyzed at days 7, 14, 21, 28, and 36 using a vibrating sample magnetometer (VSM) (Quantum Design, Versalab or PPMS). Field-dependent magnetization curves were measured at 300 K as a function of the external field. A low range of -150 to +150 mT was first performed to obtain precise measurements. A higher range of 0 to 3000 mT provided magnetization at saturation.

Each magnetization curve was fitted by Langevin law, $M(H) = m_s\phi(\coth \xi - 1/\xi)$ with $\xi = 10^{-4}M_s\pi d^3B/6kT$, B being the magnetic field, M_s the sample saturation magnetization, k the Boltzmann constant, and T the temperature. Because of nanoparticles polydispersity, the Langevin equation was weighted by the diameter lognormal distribution expressed as $P(d) = \frac{1}{(\sqrt{2\pi}\sigma d)} \times \exp\left(-\frac{\ln^2\left(\frac{d}{d_{mag}}\right)}{2\sigma^2}\right)$, with σ the polydispersity index, and d_{mag} the magnetic diameter.

Transmission Electron Microscopy (TEM)

Cells were rinsed with PBS and fixed in 5% glutaraldehyde and 0.1 mol/L sodium cacodylate buffer (Sigma-Aldrich). Post-fixation was achieved with 1% osmium tetroxide solution (Sigma) containing 1.5% potassium cyanoferrate (Sigma). Gradually dehydration was performed in ascending concentrations of ethanol and cells were embedded in Epon resin. Thin sections (70 nm) were examined with a HITACHI HT

7700 operating at 120kV (INRA, France). Size of the nanostructures was analyzed using ImageJ.

Quantitative RT-PCR

Expression level of four genes involved in iron metabolism was analyzed by RT-qPCR. Total RNA was extracted from mMSC according to the manufacturer's instructions using the NucleoSpin® RNA kit (Machery-Nagel). An incubation with 10U of DNase for 15 min was performed to avoid DNA contamination. Complementary DNA (cDNA) was then obtained by reverse transcription, using SuperScript II Reverse Transcriptase kit (Thermo Fisher Scientific) according to the manufacturer's instructions. Real-time PCR was carried out using QuantStudio3 (Applied Biosystem) and SYBR green PCR Master Mix (Applied Biosystems). Results were analyzed by the software QuantStudio. The expression of 60S acidic ribosomal protein P0 (RPLP0) was used as reference transcript and results were normalized to controls (cells without iron at day 0). The sequences of primers used are presented in Table 1.

Genes	Primers sequences (5' → 3')
RPLP0	Fwd: GCCAGCTCAGAACACTGGTCTA
	Rev: ATGCCCAAAGCCTGGAAGA
FTH1	Fwd: AAGATGGGTGCCCCTGAAG
	Rev: CCAGGGTGTGCTTGTCAAAGA
FTL1	Fwd: GAGGTCCCGTGGATCTGTGT
	Rev: GGAATCCCCGGGTCTGTT
TRF	Fwd: CTCAGTTTCCGCCATCTCAGT
	Rev: GCAGCTCTTGAGATTGTTTGCA
SLC40A1	Fwd: TCACCTGGCTACGTCGAAAAT
	Rev: GCTGGGCTAGTCCTGAGAATAGAC

Table 1: List of primer sequences for gene expression analyses by quantitative real-time PCR. RPLP0: Ribosomal protein large subunit P0; FTH1: Ferritin Heavy Chain 1; FTL1: Ferritin Light Chain 1; TRF: Transferrin; SLC40A1: Ferroportin.

X-ray Absorption Spectroscopy (XAS)

XAS measurements were performed on dry solutions of iron salt or on a pull of enough cells to have a good signal-to-noise ratio. Measurements were achieved in the X-ray absorption near edge structure (XANES) and extended X-ray absorption fine structure (*EXAFS*) regimes at the BM23 beamline of the European Synchrotron Radiation Facilities (ESRF, Grenoble, France) and at the CLÆSS beamline (BL22) of the Spanish synchrotron ALBA-CELLS (Barcelona, Spain). All spectra were acquired at room temperature and atmospheric pressure in transmission and fluorescence modes at the Fe K-edge (7112 eV). Each XAS spectrum of cells was an average accumulation of 5-10 acquisitions merged to improve the signal-to-noise ratio. The energy calibration was performed by a metal Fe foil standard. Data normalization, energy calibration, and XAS analysis were performed using the Demeter software package (Athena program).[52] XAS signal was obtained by normalizing the magnitude of the oscillations to the edge jump, removing the background with a cubic spline-fitting polynomial. Iron oxides (as maghemite and ferrihydrite) were chosen as iron oxide-based reference standards.

Statistical Analysis

Values ($n \geq 3$) are presented as mean ± standard deviation (SD). Significance between two groups was determined using independent Student's t-test. P-values were considered significant with a minimum of 95% confidence level: $*p < 0.05$, $**p < 0.01$ and $***p < 0.001$.

Figures

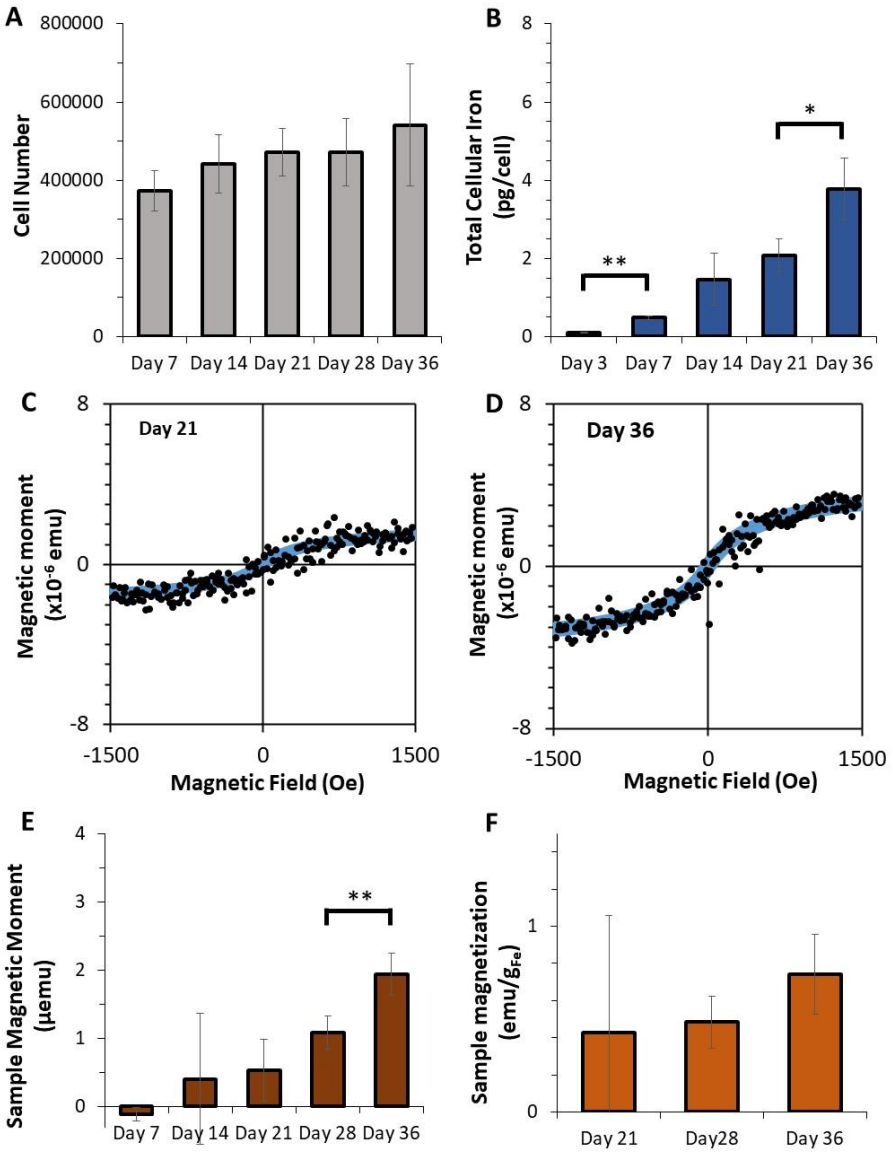

Figure 1. Iron management by mouse mesenchymal stem cells (mMSC) along continuous exposure to [Fe] = 34 µM of ferric quinate and 2 mM citrate. **A**: Number of mMSC cells progressively increase over time, an indicator of the cellular viability. **B**: ICP-AES analyses of total iron on cell bulks (200 000 cells initially), reported to total cell number, indicate an increased internalization of ferric iron over the 36 days of culture, without reaching saturation. **C,D**: Typical magnetization curves obtained by VSM for the cell bulks at days 21 (C) and 36 (D). For each curve, the fit using Langevin's formalism is superposed (blue curve), corresponding to magnetic diameter d_{mag}=6.5 nm (C) and d_{mag}=7.2 nm (D) with polydispersity index σ=0.36 (C) and σ=0.32 (D). **E,F**: Saturation magnetization was measured at each time point, for the cells samples (E, 200 000 cells at day 0) with values in the 10^{-6} emu (µemu) range or reported to total cell number (F) with values in the 10^{-12} emu (pemu) range.

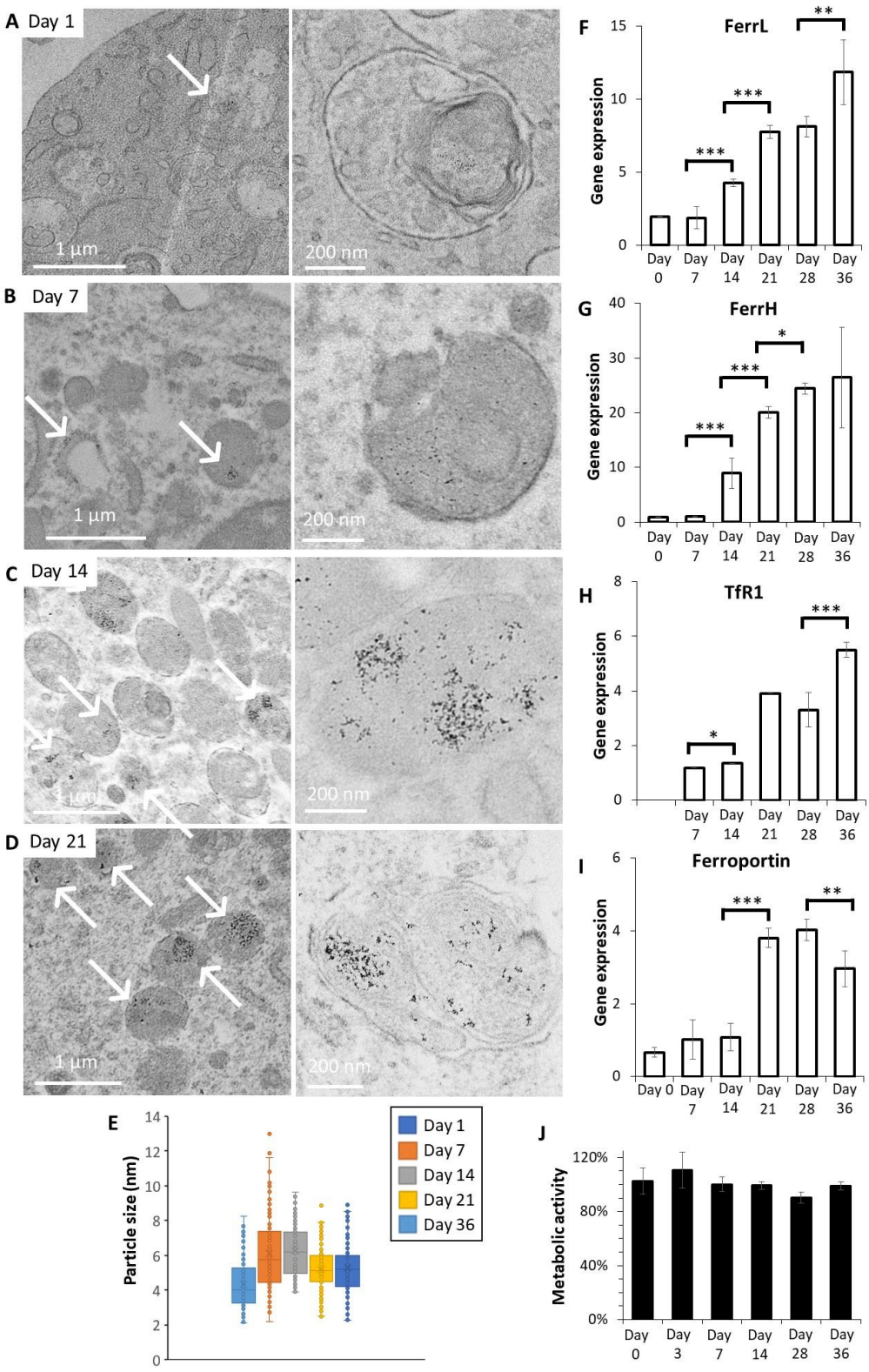

Figure 2: **A-D**: Transmission electron microscopy (TEM) images taken 1 (A), 7 (B), 14 (C), and 21 (D) days upon incubation with 34 µM ferric quinate and 2 mM citrate evidence the presence of dark dots, mostly within the endosomal compartments of the cells. **E**: Size analysis of the dark dots observed in TEM indicates an average diameter of 6 nm. **F-I**: Expression of genes coding for proteins involved in iron metabolism (storage: L-subunit of Ferritin (FerrL, F) and H-subunit of Ferritin (FerrH, G); import: Transferrin receptor protein 1 (TfR1, H); export: Ferroportin (I)), reported to RPLP0 and normalized to control cells (not incubated with iron) from day 0. **J**: Cells metabolic activity after a 24h ferric quinate incubation at 1 mM (Fe quantity of 2 pg per cell reached at day 1) over maturation time and expressed in percent of control cells (no iron).

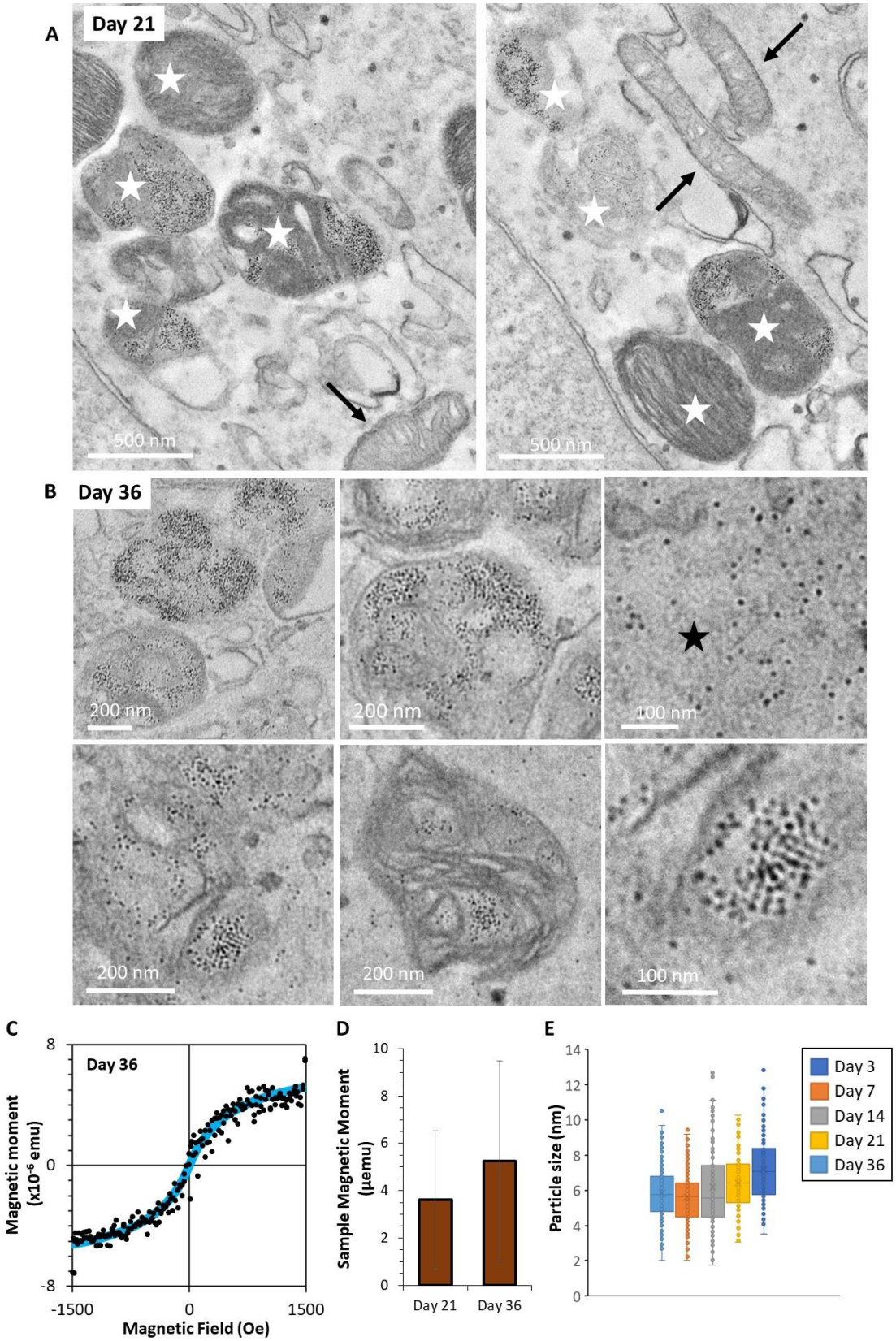

Figure 3. Magnetic biomineralization in human MSC (hMSC), along the adipogenesis differentiation pathway, and continuously incubated with 34 µM ferric quinate and 2 mM citrate. **A,B**: Representative TEM images at day 21 (A) and day 36 (B) showing dark dots typical of iron-based nanostructures. These dots are mainly located within cellular endosomes (indicated by white stars in A) and none are present in mitochondria (indicated by black arrows in A). Images in B are focused on the nanostructures, localized in the endosomes on most images,

except for one, indicated by a black star, showing nanostructures in the cytoplasm. Cytoplasm localization remains however rare. **C**: Typical magnetization curve obtained by VSM at day 36. The corresponding Langevin's fit is superposed (blue curve) and indicates a magnetic diameter d_{mag}=7.3 nm with a polydispersity index σ=0.31. **D**: Average magnetic moment measured on the whole cell content (initial seeding density at 200 000 cells). **E**: Size analysis indicates nanostructures systematically in the 6-8 nm range in diameter.

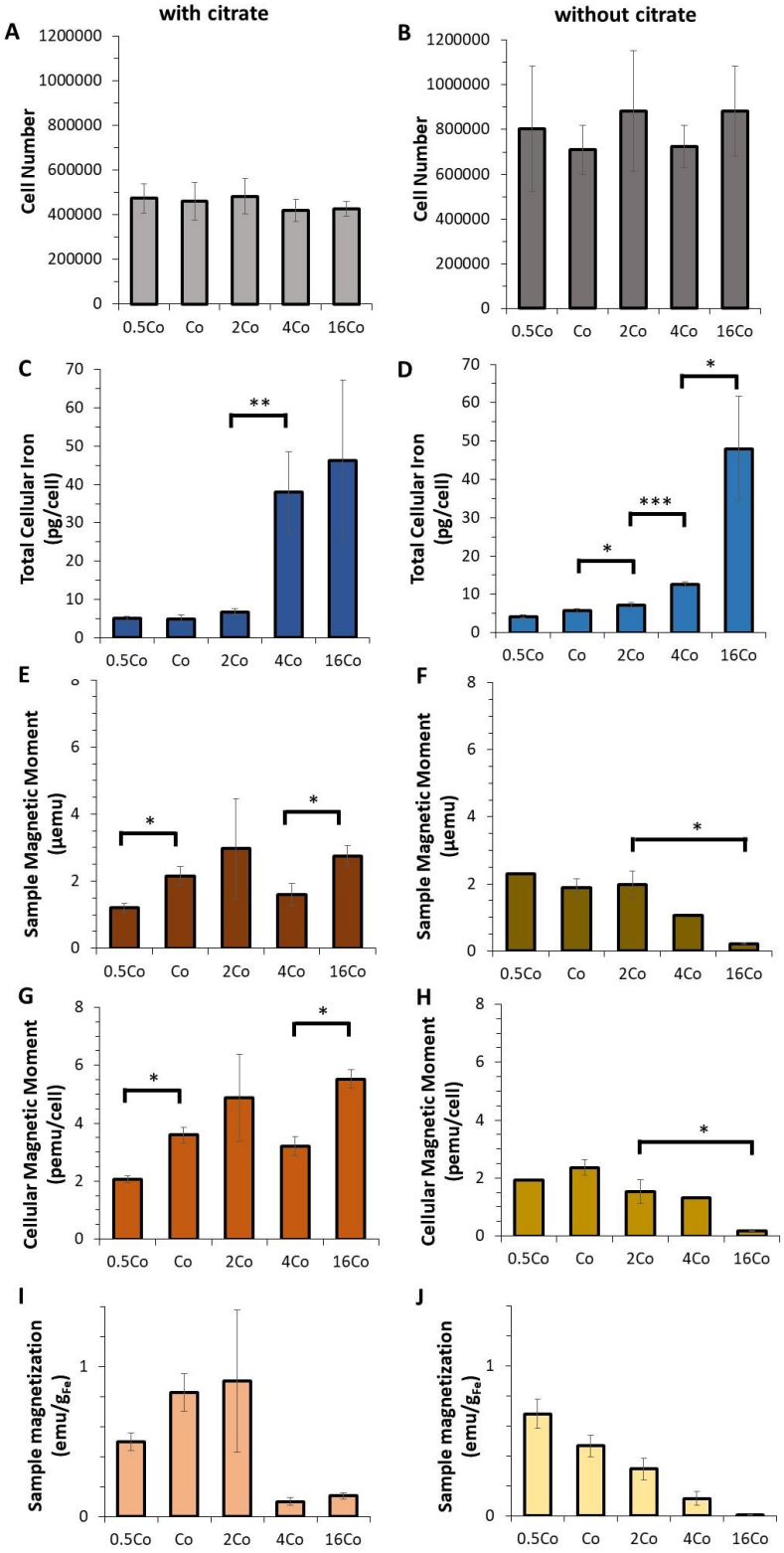

Figure 4. Management of iron by mMSC upon 36 days of continuous incubation with varying administered doses of ferric quinate (0.5C_0, C_0, 2C_0, 4C_0, or 16 C_0), with 2 mM citrate (A,C,E,G) or without (B, D, F,H). **A,B**: Total number of cells after 36 days. **C,D**: Total iron content per

cell upon 36 days of incubation. **E-H**: Average magnetic moment for the cell samples (E,F) and renormalized per cell (G,H). **I,J**: Renormalized samples magnetization expressed in emu per gram of Fe.

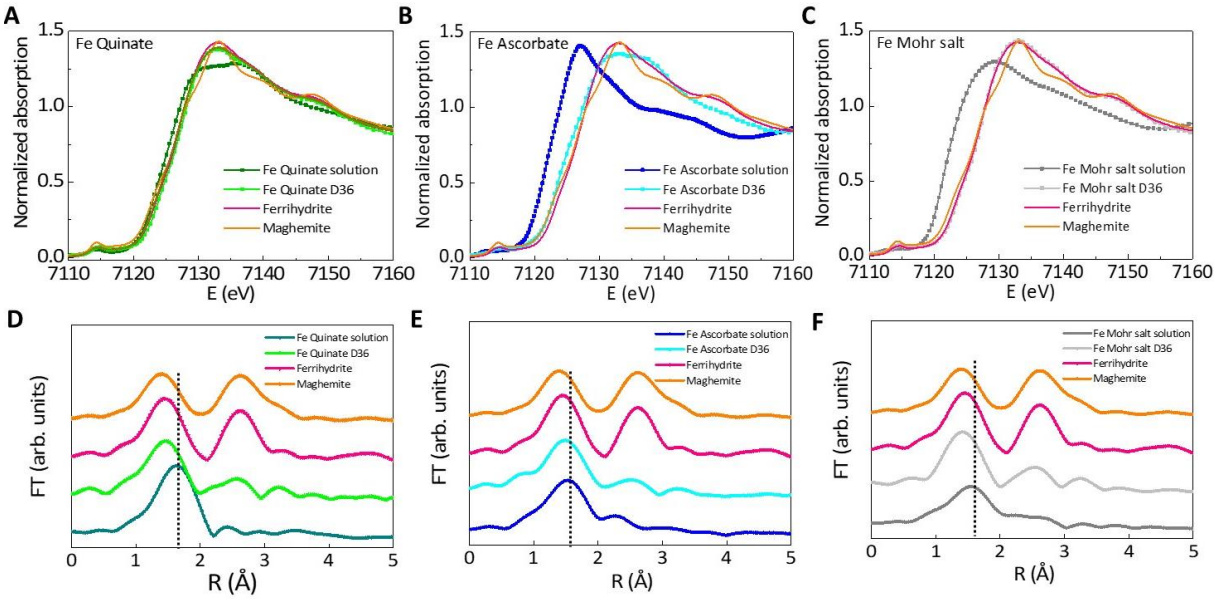

Figure 5. X-ray absorption spectroscopy (XAS) to study the evolution of different iron oxide-based nanomaterials within cells that were previously incubated for 36 days with iron salts at [Fe] = 34 µM supplemented with 2 mM citrate. **A-C**: XAS spectra at the near-edge structure (XANES) regime were measured at Fe K-edge (7112 eV) for incubation with ferric quinate (A), ferrous ascorbate (B), or Mohr's salt (C). The XANES spectra at the Fe K-edge are shown for the initial solution, for the cells at 36 days, and for ferrihydrite and maghemite references. They display a shift of energy edge of iron in cells revealing an oxidation state of 3+ (on average) that matches with the existence of different proportions of ferrihydrite and/or maghemite. Other phases based on N, C, etc. are also possible. **D-F:** k^2-weighted EXAFS spectra at the Fe K-edge. A visual guide is marked to follow the position of the first shell.

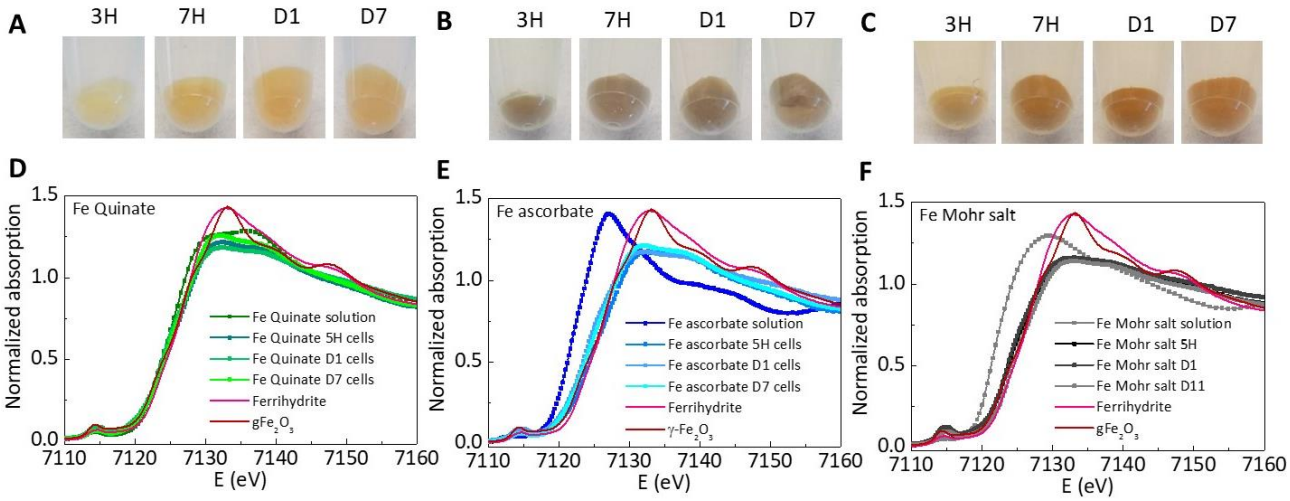

Figure 6: X-ray absorption spectroscopy (XAS) to monitor the first events of iron internalization and cell management. Cells were incubated with iron salts at [Fe] = 4 mM, supplemented with 2 mM citrate, for only 7 hours. **A-C**: Images of the cell pellets collected at 3 hours, 7 hours, one day or 7 days during or after the incubation period are shown for all salts (A, ferric quinate; B, ferrous ascorbate; C, Mohr). **D-E**: XANES spectra at the Fe K-edge are shown for ferric quinate (D), ferrous ascorbate (E) and Mohr's salt (F), for initial solutions and for incubated cells after 3 hours, 5 hours, one day or 7 days. References of ferrihydrite and maghemite are also depicted. They exhibit biotransformation in situ of the initial precursor.

Conflicts of interest

There are no conflicts to declare.

Acknowledgements

This work was supported by the European Union (ERC-2019-CoG project NanoBioMade 865629 and ERC-2022-POC1 project BioMag 101069301) and by ANR (grant ANR-19-CE09-0029). We thank Laure Cordier for the ICP-AES analyses at the Institut de Physique du Globe de Paris platform (IPGP). We thank the BM23 (ESRF, France) and CLAESS (ALBA, Spain) beamline staff for the support during the experiments. A.VdW. acknowledges support from CNRS through the MITI interdisciplinary programs (Métallo-Mix project, BioMAG). A.E. acknowledges the financial support from Comunidad de Madrid (2018-T1/IND-1005 project, and Spanish MICIN (RYC2021-031236-I (A. S.) and RYC2020-029282-I (A. E.).

References

1. M. A. Zoroddu, J. Aaseth, G. Crisponi, S. Medici, M. Peana and V. M. Nurchi, *Journal of inorganic biochemistry*, 2019, **195**, 120-129.
2. J. Liu, S. Chakraborty, P. Hosseinzadeh, Y. Yu, S. Tian, I. Petrik, A. Bhagi and Y. Lu, *Chemical reviews*, 2014, **114**, 4366-4469.
3. H. Naatz, B. B. Manshian, C. Rios Luci, V. Tsikourkitoudi, Y. Deligiannakis, J. Birkenstock, S. Pokhrel, L. Mädler and S. J. Soenen, *Angewandte Chemie*, 2020, **132**, 1844-1852.
4. R. Hachani, M. A. Birchall, M. W. Lowdell, G. Kasparis, L. D. Tung, B. B. Manshian, S. J. Soenen, W. Gsell, U. Himmelreich and C. A. Gharagouzloo, *Scientific Reports*, 2017, **7**, 1-14.
5. S. Harvell-Smith and N. T. K. Thanh, *Nanoscale*, 2022, **14**, 3658-3697.
6. S. Sharma, N. Shrivastava, F. Rossi and N. T. K. Thanh, *Nano Today*, 2019, **29**, 100795.
7. S. Kralj and S. Marchesan, *Pharmaceutics*, 2021, **13**, 1262.
8. G. Mandriota and R. Di Corato, *Magnetic Nanoparticles in Human Health and Medicine: Current Medical Applications and Alternative Therapy of Cancer*, 2021, 59-86.
9. R. Di Corato, A. Aloisi, S. Rella, J.-M. Greneche, G. Pugliese, T. Pellegrino, C. Malitesta and R. Rinaldi, *ACS applied materials & interfaces*, 2018, **10**, 20271-20280.
10. M.-S. Martina, C. Wilhelm and S. Lesieur, *Biomaterials*, 2008, **29**, 4137-4145.
11. V. Garcés, A. González, N. Gálvez, J. M. Delgado-López, J. J. Calvino, S. Trasobares, Y. Fernández-Afonso, L. Gutiérrez and J. M. Dominguez-Vera, *Nanoscale*, 2022, **14**, 5716-5724.
12. H. Gavilán, K. Simeonidis, E. Myrovali, E. Mazarío, O. Chubykalo-Fesenko, R. Chantrell, L. Balcells, M. Angelakeris, M. P. Morales and D. Serantes, *Nanoscale*, 2021, **13**, 15631-15646.
13. N. Silvestri, H. Gavilán, P. Guardia, R. Brescia, S. Fernandes, A. C. S. Samia, F. J. Teran and T. Pellegrino, *Nanoscale*, 2021, **13**, 13665-13680.
14. H. Gavilán, G. M. Rizzo, N. Silvestri, B. T. Mai and T. Pellegrino, *Nature Protocols*, 2023, 1-27.
15. J. L. Kirschvink, A. Kobayashi-Kirschvink and B. J. Woodford, *Proceedings of the National Academy of Sciences*, 1992, **89**, 7683-7687.
16. S. A. Gilder, M. Wack, L. Kaub, S. C. Roud, N. Petersen, H. Heinsen, P. Hillenbrand, S. Milz and C. Schmitz, *Scientific reports*, 2018, **8**, 1-9.
17. T. Gonet and B. A. Maher, *Environmental Science & Technology*, 2019, **53**, 9970-9991.
18. P. P. Schultheiss-Grassi, R. Wessiken and J. Dobson, *Biochimica et Biophysica Acta (BBA)-General Subjects*, 1999, **1426**, 212-216.
19. A. Van de Walle, A. Plan Sangnier, A. Abou-Hassan, A. Curcio, M. Hémadi, N. Menguy, Y. Lalatonne, N. Luciani and C. Wilhelm, *Proceedings of the National Academy of Sciences*, 2019.
20. A. Curcio, A. Van de Walle, A. Serrano, S. Preveral, C. Péchoux, D. Pignol, N. Menguy, C. T. Lefevre, A. Espinosa and C. Wilhelm, *ACS nano*, 2019, **14**, 1406-1417.
21. P. Singh, Y.-J. Kim, D. Zhang and D.-C. Yang, *Trends in biotechnology*, 2016, **34**, 588-599.
22. M. Kitching, M. Ramani and E. Marsili, *Microbial biotechnology*, 2015, **8**, 904-917.
23. I. Shukurov, M. S. Mohamed, T. Mizuki, V. Palaninathan, T. Ukai, T. Hanajiri and T. Maekawa, *International Journal of Molecular Sciences*, 2022, **23**, 2292.
24. A. Nanda and M. Saravanan, *Nanomedicine: Nanotechnology, Biology and Medicine*, 2009, **5**, 452-456.
25. D. Faivre and D. Schuler, *Chemical reviews*, 2008, **108**, 4875-4898.
26. S. Kaushik, J. Thomas, V. Panwar, P. Murugesan, V. Chopra, N. Salaria, R. Singh, H. S. Roy, R. Kumar, V. Gautam and D. Ghosh, *Nanoscale*, 2022, **14**, 1713-1722.
27. A. Pekarsky and O. Spadiut, *Frontiers in Bioengineering and Biotechnology*, 2020, **8**, 573183.
28. E. Firlar, M. Ouy, A. Bogdanowicz, L. Covnot, B. Song, Y. Nadkarni, R. Shahbazian-Yassar and T. Shokuhfar, *Nanoscale*, 2019, **11**, 698-705.
29. I. Orue, L. Marcano, P. Bender, A. García-Prieto, S. Valencia, M. A. Mawass, D. Gil-Cartón, D. Alba Venero, D. Honecker, A. García-Arribas, L. Fernández Barquín, A. Muela and M. L. Fdez-Gubieda, *Nanoscale*, 2018, **10**, 7407-7419.
30. A. Peigneux, Y. Jabalera, M. A. F. Vivas, S. Casares, A. I. Azuaga and C. Jimenez-Lopez, *Scientific Reports*, 2019, **9**, 8804.
31. A. Elfick, G. Rischitor, R. Mouras, A. Azfer, L. Lungaro, M. Uhlarz, T. Herrmannsdörfer, J. Lucocq, W. Gamal and P. Bagnaninchi, *Scientific reports*, 2017, **7**, 39755.
32. S.-W. Lee, S.-H. Lee and S. Biswal, *Theranostics*, 2012, **2**, 403.
33. O. Zurkiya, A. W. Chan and X. Hu, *Magnetic Resonance in Medicine: An Official Journal of the International Society for Magnetic Resonance in Medicine*, 2008, **59**, 1225-1231.
34. J. Wang, G. Zhang, Q. Li, H. Jiang, C. Liu, C. Amatore and X. Wang, *Scientific reports*, 2013, **3**, 1157.
35. T. Du, C. Zhao, F. ur Rehman, L. Lai, X. Li, Y. Sun, S. Luo, H. Jiang, M. Selke and X. Wang, *Nano Research*, 2017, **10**, 2626-2632.
36. L. Lai, C. Zhao, X. Li, X. Liu, H. Jiang, M. Selke and X. Wang, *RSC Advances*, 2016, **6**, 30081-30088.
37. T. Du, C. Zhao, F. ur Rehman, L. Lai, X. Li, Y. Sun, S. Luo, H. Jiang, N. Gu, M. Selke and X. Wang, *Advanced Functional Materials*, 2017, **27**, 1603926.

38. Y. Noguchi, T. Fujiwara, K. Yoshimatsu and Y. Fukumori, *Journal of bacteriology*, 1999, **181**, 2142-2147.
39. Z. Yuan, B. Wang, Y. Teng, W. Ho, B. Hu, K. O. Boakye-Yiadom, X. Xu and X.-Q. Zhang, *Nanoscale*, 2022, **14**, 6449-6464.
40. A. González, O. Pokrovsky, F. Jiménez-Villacorta, L. Shirokova, J. Santana-Casiano, M. González-Dávila and E. Emnova, *Chemical Geology*, 2014, **372**, 32-45.
41. A. Espinosa, A. Serrano, A. Llavona, J. J. De La Morena, M. Abuin, A. Figuerola, T. Pellegrino, J. Fernández, M. Garcia-Hernandez and G. Castro, *Measurement Science and Technology*, 2011, **23**, 015602.
42. J. Shaw, A. Boyd, M. House, R. Woodward, F. Mathes, G. Cowin, M. Saunders and B. Baer, *Journal of The Royal Society Interface*, 2015, **12**, 20150499.
43. H. Sant'Ovaia, G. Marques, A. Santos, C. Gomes and A. Rocha, *Biometals*, 2015, **28**, 951-958.
44. F. Brem, A. M. Hirt, M. Winklhofer, K. Frei, Y. Yonekawa, H.-G. Wieser and J. Dobson, *Journal of The Royal Society Interface*, 2006, **3**, 833-841.
45. C. X. Wang, I. A. Hilburn, D.-A. Wu, Y. Mizuhara, C. P. Cousté, J. N. Abrahams, S. E. Bernstein, A. Matani, S. Shimojo and J. L. Kirschvink, *eneuro*, 2019.
46. D. Galante, E. Cavallo, A. Perico and C. D'Arrigo, *Biopolymers*, 2018, **109**, e23224.
47. C. Caiazza, M. D'Agostino, F. Passaro, D. Faicchia, M. Mallardo, S. Paladino, G. M. Pierantoni and D. Tramontano, *International Journal of Molecular Sciences*, 2019, **20**, 2613.
48. T.-A. Wang, S.-L. Xian, X.-Y. Guo, X.-D. Zhang and Y.-F. Lu, *Oncology Reports*, 2018, **39**, 271-279.
49. K. Fan, C. Cao, Y. Pan, D. Lu, D. Yang, J. Feng, L. Song, M. Liang and X. Yan, *Nature nanotechnology*, 2012, **7**, 459-464.
50. C. Cao, L. Tian, Q. Liu, W. Liu, G. Chen and Y. Pan, *Journal of Geophysical Research: Solid Earth*, 2010, **115**.
51. C. Piquer, M. Laguna-Marco, A. G. Roca, R. Boada, C. Guglieri and J. Chaboy, *The Journal of Physical Chemistry C*, 2014, **118**, 1332-1346.
52. B. Ravel and M. Newville, *Journal of synchrotron radiation*, 2005, **12**, 537-541.